Supporting Information

to

Target Profiling of an Antimetastatic RAPTA Agent by Chemical Proteomics: Relevance to the Mode of Action

Maria V. Babak,[a,b] Samuel M. Meier,[c] Kilian Huber,[d] Jóhannes Reynisson,[a] Anton A. Legin,[b] Michael A. Jakupec,[b] Alexander Roller,[b] Alexey Stukalov,[d] Manuela Gridling,[d] Keiryn L. Bennett,[d] Jacques Colinge,[d] Walter Berger,[e] Paul J. Dyson,[f] Giulio Superti-Furga,[d] Bernhard K. Keppler,[b] Christian G. Hartinger*[a]

[a] School of Chemical Sciences, University of Auckland, Private Bag 92019, Auckland 1142, New Zealand

[b] Institute of Inorganic Chemistry, University of Vienna, Waehringer Str. 42, A-1090 Vienna, Austria

[c] Institute of Analytical Chemistry, University of Vienna, Waehringer Str. 38, A-1090 Vienna, Austria

[d] CeMM Research Center for Molecular Medicine, Lazarettgasse 14, AKH BT 25.3, A-1090 Vienna, Austria

[e] Department of Medicine I, Institute of Cancer Research, Medical University Vienna, Borschkegasse 8a, A-1090 Vienna, Austria

[f] Institut des Sciences et Ingénierie Chimiques, Ecole Polytechnique Fédérale de Lausanne, CH-1015 Lausanne, Switzerland

Table of Contents

Experimental Details

Materials and Methods. Materials from chemical suppliers were used as received and all the reactions were carried out under argon atmosphere in anhydrous solvents. $RuCl_3 \cdot 3H_2O$ was purchased from Johnson Matthey. $[(\eta^6\text{-Benzylammonium})RuCl_2]_2Cl_2$ (**a**),[1] 1,4-cyclohexadiene-1-methanamine (**b**),[2] and 1,3,5-triaza-7-phosphaadamantane (PTA)[3] were prepared according to literature procedures. Methanol was dried and distilled over Mg under an argon atmosphere. D-Biotin and 6-biotinylamino-hexanoic acid-*N*-hydroxysuccinimidyl ester were purchased from Iris Biotech GMBH, triethylamine (99%) and dimethylsulfoxide (p.a.) from Acros, acetic anhydride (≥99.0%) and ethanolamine (p.a.) from Fluka, N,N-dimethyl formamide (absolute, over molecular sieves, ≥99.5%) from Aldrich, sodium dodecyl sulphate (≥98.5%), HEPES (99.5%), ubiquitin (from bovine erythrocytes) and horse heart cytochrome-c were from Sigma and tetramethylammonium acetate (>98%) from TCI. The isolation of products was conducted without any special precautions. Elemental analyses were performed by the Microanalytical Laboratory of the Faculty of Chemistry of the University of Vienna. Electrospray ionization mass spectrometry was carried out with a Bruker Esquire 3000 instrument (Bruker Daltonics, Bremen, Germany), MilliQ water (18.2 MΩ; Millipore Synergy 185 UV Ultrapure Water System; Molsheim, France) and methanol (VWR Int., HiPerSolv, CHROMANORM) were used as solvents for ESI-MS studies. The ^1H and ^{31}P NMR spectra were recorded at 500.10 and 202.44 MHz on a Bruker FT-NMR spectrometer Avance IITM 500 MHz. ^1H NMR kinetic experiments were measured at 500.32 MHz on a Bruker DPX500 (Ultrashield Magnet). Chemical shifts are given in ppm relative to the residual solvent peak.

X-ray Diffraction Analysis. X-ray diffraction measurements were performed on a Bruker X8 APEX II CCD diffractometer at 100 K. Single crystals were positioned at 35 mm from the detector, and 1112 and 2123 frames were measured, each for 60 and 20 s over 1° scan width for **1** and **3**, respectively. The data were processed using SAINT software.[4] Crystal data, data collection parameters, and structure refinement details for 1 and 3 are given in Table S1 and key bond lengths and angles in Table S2. The structures were solved by direct methods and refined by full-matrix least-squares techniques. Non-hydrogen atoms were refined with anisotropic displacement parameters. H atoms were placed at calculated positions and refined as riding atoms in the subsequent least squares model refinements. The isotropic thermal parameters were estimated to be 1.2 times the values of the equivalent isotropic thermal parameters of the non-hydrogen atoms to which hydrogen atoms are bonded. The following computer programs, equipment and tables were used: structure solution, SHELXS-97; refinement, SHELXL-2013,[5] OLEX2;[6] molecular diagrams, Mercury 3.0.

Cell Lines and Culture Conditions. The human cancer cell lines CH1 (ovarian carcinoma), A549 (non-small cell lung cancer) and SW480 (colon carcinoma) were grown in 75 cm^2 culture flasks (CytoOne, Starlab, UK) as adherent monolayer cultures in complete medium [*i.e.*, Minimal Essential Medium (MEM) supplemented with 10% heat-inactivated fetal bovine serum, 1 mM sodium pyruvate, 4 mM L-glutamine, and 1% from 100x nonessential amino acids ready-to-use stock (all purchased from Sigma-Aldrich Austria)]. Cell cultures were incubated at 37 °C in a moist atmosphere containing 5% CO_2.

Cytotoxicity in Cancer Cell Lines. The cytotoxicity of the compounds was determined by means of colorimetric microculture assay (MTT assay, MTT = 3-(4,5-dimethyl-2-thiazolyl)-2,5-diphenyl-2H-tetrazolium bromide). The cells were harvested from culture flasks by trypsinization and seeded into 96-well microculture plates (CytoOne, Starlab, UK) in densities of 1×10^3 cells per well (for CH1), 2.5×10^3 cells per well (for SW480) and 3×10^3 cells per well (for A549). After 24 h preincubation of the cells, the test compounds were dissolved in complete medium and then added in aliquots of 100 µL per well. After continuous exposure for 96 h, solutions of the compounds were replaced with 86 µL RPMI 1640 medium (supplemented with 10% heat-inactivated fetal bovine serum and 2 mM L-glutamine) plus 14 µL MTT solution in phosphate-buffered saline (5 mg/mL). After incubation for 4 h, the medium/MTT mixtures were removed, and the formazan crystals formed by viable cells were dissolved in 150 µL of DMSO per well. Optical densities at 550 nm were measured with a microplate reader (ELx808 Absorbance Microplate Reader, Bio-Tek, USA), using a reference wavelength of 690 nm to correct for unspecific absorption. The quantity of viable cells was expressed in terms of T/C values by comparison to untreated control microcultures, and 50% inhibitory concentrations (IC_{50}) were calculated from concentration-effect curves by interpolation. Evaluation is based on means from at least three independent experiments, each comprising three replicates per concentration level.

Stability Studies. Stability studies for 1 were performed on an AmaZon SL ion trap mass spectrometer using ESI Compass 1.3 software (Bruker Daltonics GmbH, Bremen, Germany). The samples were introduced by direct infusion at a flow rate of 180 µL/h. Compound **1** was dissolved in dimethylsulfoxide or dry N,N-dimethylformamide, respectively, and was incubated for the appropriate time. The sample was diluted with water : methanol (1 : 1) to a final concentration of 5 µM prior to injection into the instrument. Typical instrument parameters were as follows: average accumulation time ~1500 µs, dry gas 6.0 L/min, dry temperature 100 °C, end plate offset –500 V, HV capillary –3.5 kV, nebulizer 8 psi, RF Level 63%, trap drive 55.2. The Data Analysis 4.0 software package (Bruker Daltonics GmbH, Bremen, Germany) was used for processing of the raw data. Stability studies in aqueous solution were carried out as described below.

Protein Binding Studies. Compounds **1** or **3** (400 µM) and ubiquitin or cytochrome-c (400 µM) were dissolved in water and tetramethylammonium acetate (20 mM). These stock solutions were mixed to obtain a 2 : 1 metal-to-ubiquitin and a 3 : 1 metal-to-cytochrome-c molar ratio. The final protein concentration was 50 µM and the mixtures were incubated at 37 °C in the dark using a thermomixer at 400 rpm (Ditabis, Pforzheim, Germany, HLC). References containing only **1** or **3** (50 µM) were incubated in parallel. Mass spectra of the incubation solutions were recorded after 2, 6, 24 and 48 h. The samples were analyzed using a MaXis Q-ToF mass spectrometer (Bruker Daltonics, Bremen, Germany) equipped with a Triversa nanomate (Advion Biosystems Inc., Ithaca, New York, USA) using ChipSoft 8.3 (Advion Biosystems Inc.) to control the nanomate. The general parameters were as follows: HV capillary –1.8 kV, gas flow 0.1 psi, dry temperature 180 °C, 200 Vpp funnel RF, 3 eV quadrupole ion energy, 150 µs ion cooler transfer time and 15 °C nanomate sample plate temperature. The samples were diluted before injection to 1–3 µM using water : methanol : formic acid (50 : 50 : 0.2). The spectra were recorded in positive ion mode over 0.5 min and averaged. The Data Analysis 4.0 software package was used for processing and maximum entropy deconvolution (automatic data point spacing and 30000 instrument resolving power) was applied. Relative abundances of adducts are expressed as percentage of the signal intensity of all assigned adducts with respect to the signal intensity of all assigned mass signals in the deconvoluted sprectrum.

Docking Experiments. The structures were docked to a streptavidin crystal structure (3RY2, resolution 0.95 Å),[7] which was obtained from the Protein Data Bank (PDB).[8, 9] The Scigress Ultraversion 7.7.0.47 program[10] was used to prepare the crystal structure for docking, *i.e.* hydrogen atoms were added, the co-crystallized ligand (biotin) was removed as well as crystallographic water molecules. The Scigress software suite was also used to build the compounds and the MM2[11] force field was used to optimize the structures. The center of the binding pocket was defined as the oxygen atom on the bicyclic system (x = 27.048, y = 10.773, z = 12.293) in biotin with 10 Å radius. Fifty docking runs were allowed for each ligand with default search efficiency (100%). The basic amino acids lysine and arginine were defined as protonated. Furthermore, aspartic and glutamic acids were assumed to be deprotonated. All the bonds to the metal centre were fixed for the docking runs. The GoldScore (GS),[12] ChemScore (CS),[13, 14] ChemPLP[15] and ASP[16] algorithms in the GOLD v5.1 software suite were implemented to predict binding modes and relative energies of the ligands.

Drug Pull-Down. For preparation of cell lysates, CH1 cells (see above) were lysed with lysis buffer (50 mM Tris–HCl, 100 mM NaCl, 0.2% NP-40, 5% glycerol, 1.5 mM $MgCl_2$, 25 mM NaF, 1 mM Na_3VO_4, 1 mM phenylmethylsulfonyl fluoride, 1 mM dithiothreitol (DTT), 10 µg/mL TLCK, 1 µg/mL leupeptin, 1 µ g/mL aprotinin, and 10 µg/mL soybean trypsin inhibitor (Sigma), pH 7.5). Per pull-down experiment, 100 µL streptavidin bead slurry (UltraLink Immobilized Streptavidin Plus, 50% in 20% ethanol, Pierce)

was distributed in Eppendorf tubes, centrifuged, and the supernatant removed. After washing with lysis buffer (3 × 1 mL), 50 mmol of biotin-conjugated compound **3** was added (prepared as described below) and incubated on a roto-shaker for 30 min at 4 °C. After centrifugation and one additional washing step, the beads were resuspended in CH1 lysates (10 mg per pull-down) and incubated on a roto-shaker for 2 h at 4 °C. For competition experiments, lysates were preincubated with 20 µM of 2 for 20 min at 4 °C. After centrifugation, beads were transferred to spin columns (MoBiTec) and washed with lysis buffer (5 mL) and HEPES (2.5 mL), respectively. To elute bound proteins, the beads were treated with 250 µL elution buffer (3 M urea, 50 mM formic acid) and the eluates were collected in glass vials.

Liquid chromatography-mass spectrometry. Mass spectrometry was performed on a hybrid LTQ Orbitrap Velos mass spectrometer (ThermoFisher Scientific, Waltham, MA, USA) using Xcalibur version 2.1.0 SP1.1160 coupled to an Agilent 1200 HPLC nanoflow system (dual pump with one precolumn and one analytical column; Agilent Biotechnologies, Palo Alto, CA, USA) via a nanoelectrospray ion source using liquid junction (Proxeon, Odense, Denmark). Solvents for HPLC separation of peptides were as follows: solvent A consisted of 0.4% formic acid (FA) in water and solvent B consisted of an aqueous solution of 0.4% FA in 70% methanol and 20% isopropanol. From a thermostatted microautosampler, 8 µL of the tryptic peptide mixture was automatically loaded onto a trap column (Zorbax 300SB-C18 5 µm, 5 × 0.3 mm, Agilent Biotechnologies, Palo Alto, CA, USA) with a binary pump at a flow rate of 45 µL/min. 0.1% trifluoroacetic acid (TFA) used for loading and washing the precolumn. After washing, the peptides were eluted by back-flushing onto a 16 cm fused silica analytical column with an inner diameter of 50 µm packed with C18 reversed phase material (ReproSil-Pur 120 C18-AQ, 3 µm, Dr. Maisch GmbH, Ammerbuch-Entringen, Germany). The peptides were eluted from the analytical column with a 27 min gradient ranging from 3 to 30% solvent B, followed by a 25 min gradient from 30 to 70% solvent B and, finally, a 7 min gradient from 70 to 100% solvent B at a constant flow rate of 100 nL/min.[17] The analyses were performed in a data-dependent acquisition mode and dynamic exclusion for selected ions was 60 s. A top 15 collision-induced dissociation (CID) method was used, and a single lock mass at m/z 445.120024 ($Si(CH_3)_2O)_6$) was employed.[18, 19] Maximal ion accumulation time allowed in CID mode was 50 ms for MS^n in the LTQ and 500 ms in the C-trap. Automatic gain control was used to prevent overfilling of the ion traps and was set to 5000 in MSn mode for the LTQ and 10^6 ions for a full FTMS scan. Intact peptides were detected in the Orbitrap Velos at 60000 resolution at *m/z* 400. All samples were analyzed as biochemical and technical duplicates.

Data analysis. The acquired raw MS data files were processed with msconvert (ProteoWizard Library v2.1.2708) and converted into Mascot generic format (mgf) files. The resultant peak lists were searched against the human SwissProt database version v2012.05_20120529 (36898 sequences, respectively, including isoforms, as obtained from varsplic.pl) with the search engines Mascot (v2.3.02, MatrixScience, London, UK) and Phenyx (v2.5.14, GeneBio, Geneva, Switzerland).[19] Submission to the search engines

was via a Perl script that performs an initial search with relatively broad mass tolerances (Mascot only) on both the precursor and fragment ions (±10 ppm and ±0.6 Da, respectively). High-confidence peptide identifications were used to recalibrate all precursor and fragment ion masses prior to a second search with narrower mass tolerances (±4 ppm and ±0.3 Da). One missed tryptic cleavage site was allowed. Carbamidomethyl cysteine was set as a fixed modification and oxidized methionine was set as a variable modification. To validate the proteins, Mascot and Phenyx output files were processed by internally-developed parsers. Proteins with ≥2 unique peptides above a threshold score T1, or with a single peptide above a score T2 were selected as unambiguous identifications. Additional peptides for these validated proteins with score >T3 were also accepted. For Mascot and Phenyx, T1, T2 and T3 peptide scores were equal to 16, 40, 10 and 5.5, 9.5, 3.5, respectively (P-value <0.001). The validated proteins retrieved by the two algorithms were merged, any spectral conflicts discarded and grouped according to shared peptides. A false positive detection rate (FDR) of <1% and <0.1% (including the peptides exported with lower scores) was determined for proteins and peptides, respectively, by applying the same procedure against a reversed database.

Syntheses

Synthesis of [(η^6-benzylammonium)$RuCl_2$(PTA)] chloride (1). [(η^6-Benzylammonium)$RuCl_2$]$_2Cl_2$ (**a**) (0.35 mmol, 221 mg) and PTA (0.98 mmol, 157 mg) were suspended in dry DMF (30 ml) and the mixture was stirred for 4 h. An orange precipitate formed, which was collected by filtration, washed with dichloromethane and diethyl ether and dried *in vacuo* (yield: 208 mg, 63%). Crystals suitable for X-ray diffraction analysis (red needles) were grown by slow diffusion of diethyl ether into a dry methanol solution. Calc. for $C_{13}H_{22}Cl_3N_4PRu$ (472.74 g/mol): C, 33.03; H, 4.69; N, 11.85. Found: C, 33.02; H, 4.53; N, 11.47%. nESI-Q-TOF MS pos. mode: m/z 401.0230 [$RuCl(\eta^6$-$C_6H_5(CH_2)NH_2)(PTA)]^+$, 436.9987 [$RuCl_2(\eta^6$-$C_6H_5(CH_2)NH_2)(PTA) + H]^+$; found 401.0230 (<1 ppm), 436.9994 (2 ppm). ^{1}H NMR (500.10 MHz, DMSO-d^6): 8.39 (brs, 3H, NH3), 5.98 (brs, 4H, η^6-phenyl-H), 5.49 (brs, 1H, η^6-phenyl-H), 4.46 (s, 6H, PTA-CH_2), 4.23 (s, 6H, PTA-CH_2), 3.73 (brs, 2H, -CH_2-NH). $^{31}P\{^1H\}$ NMR (202.44 MHz; DMSO-d^6): -30.8 (s) ppm.

Synthesis of biotin derivative (2). Compound **1** (4.72 mg, 0.01 mmol) and 6-biotinylamino-hexanoic acid-*N*-hydroxysuccinimidyl ester (4.55 mg, 0.01 mmol) were suspended in dry DMF (2 ml). After addition of triethylamine (500 µl) and subsequent sonication the mixture was stirred for 24 h, which resulted in a clear red-brown solution. The solution was freeze-dried and *in situ* incubated with the beads. nESI-Q-TOF MS pos. mode: m/z 704.2047 [$Ru\{\eta^6$-$C_6H_5(CH_2)NH$(linker-biotin)$\}$(PTA) – H]$^+$, 722.2146 [$Ru\{\eta^6$-$C_6H_5(CH_2)NH$(linker-biotin)$\}$(PTA) + OH]$^+$, 740.1821 [$RuCl\{\eta^6$-$C_6H_5(CH_2)NH$(linker-

biotin)}(PTA)]$^+$, 776.1580 [$RuCl_2${η^6-$C_6H_5(CH_2)$NH(linker-biotin)}(PTA) + H]$^+$; found 704.2087 (6 ppm), 722.2193 (7 ppm), 740.1851 (4 ppm), 776.1615 (5 ppm).

Synthesis of *N*-(cyclohexa-1,4-dienylmethyl)acetamide (c). The synthetic method was adapted from a reported procedure.[20] Upon addition of sodium dodecyl sulfate (47 mg, 0.163 mmol) to a stirred heterogeneous suspension of 1-methylamine-1,4-cyclohexadiene (**b**) (1472 mg, 13.5 mmol) in water (30 ml), a turbid colorless solution formed. Acetic anhydride (1652 mg, 1.52 ml, 16.2 mmol) was added dropwise to the solution over a period of 40 min. It was left at 0 °C overnight and a white precipitate formed which was collected by filtration, washed with a minimal amount of diethyl ether and dried in vacuo. The solution was extracted with ethyl acetate (2 × 30 ml) and the combined organic extracts were dried with Na_2SO_4. The solvent was removed on a rotary evaporator under reduced pressure resulting in a yellow oil. It was washed with a minimal amount of diethyl ether and dried *in vacuo* to yield a white powder (yield: 1182 mg, 58%). The product was used without additional purification. ^{1}H NMR (500.10 MHz, $CDCl_3$): 5.73 (m, 2H, cyclohexadiene-CH=), 5.61 (brs, 1H, cyclohexadiene-CH=), 5.46 (m, 1H, -CONH), 3.80 (d, 2H, -CH_2-NH, $^3J_{H,H}$ = 5.8 Hz), 2.72 (m, 2H, cyclohexadiene-CH_2), 2.64 (m, 2H, cyclohexadiene-CH_2), 2.03 (s, 3H, -CH_3).

Synthesis of [(η^6-*N*-benzylacetamide)$RuCl_2$]$_2$ (d). $RuCl_3 \cdot 3H_2O$ (863 mg, 4.15 mmol) was refluxed in dry methanol (50 ml) for 40 minutes. *N*-(Cyclohexa-1,4-dienylmethyl)acetamide (**c**) (1104 mg, 7.26 mmol) was added to the clear red-brown solution and the mixture was refluxed for 18 h at 80 °C. The dark brown solution turned initially bright green and then light orange, and eventually a brown-orange precipitate formed. The solution was filtered, washed with dichloromethane and diethyl ether and dried *in vacuo* to afford an orange powder (yield: 1172 mg, 88%). The product was used without additional purification. ^{1}H NMR (500.10 MHz, DMSO-d^6): 8.34 (t, 1H, -CONH, $^3J_{H,H}$ = 5.9 Hz), 6.05 (t, 2H, η^6-phenyl-H, $^3J_{H,H}$ = 5.9 Hz), 5.82 (d, 2H, η^6-phenyl-H, $^3J_{H,H}$ = 5.6 Hz), 5.80 (t, 1H, η^6-phenyl-H, $^3J_{H,H}$ = 5.6 Hz), 4.12 (d, 2H, -CH_2-NH, $^3J_{H,H}$ = 5.9 Hz), 1.88 (s, 3H, -CH_3).

Synthesis of [(η^6-*N*-benzylacetamide)$RuCl_2$(PTA)] (3). [(η^6-*N*-Benzylacetamide)$RuCl_2$]$_2$ (**d**) (64 mg, 0.1 mmol) and PTA (47 mg, 0.3 mmol) were suspended in dry DMF (30 ml) and the mixture was stirred for 3 h. The resulting red-brown solution was filtered and the solvent was subsequently removed *in vacuo*. The remaining solid was washed with dichloromethane and diethyl ether and dried *in vacuo* (yield: 96 mg, 47%). Crystals suitable for X-ray diffraction analysis (red needles) were grown by slow diffusion of diethyl ether into a dry methanol solution. Calc. for $C_{15}H_{23}Cl_2N_4PORu$ (478.32 g/mol): C, 37.67; H, 4.85; N, 11.71. Found: C, 37.39; H, 4.49; N, 11.33%. nESI-Q-TOF MS pos. mode: m/z 443.0331 [$RuCl(\eta^6$-$C_6H_5(CH_2)NHCOCH_3)$(PTA)]$^+$, 479.0090 [$RuCl_2(\eta^6$-$C_6H_5(CH_2)NHCOCH_3)$(PTA) + H]$^+$;

found 443.0337 (1 ppm), 479.0101 (2 ppm). ^{1}H NMR (500.10 MHz, DMSO-d^{6}): 8.30 (t, 1H, -CONH , $^{3}J_{H,H}$ = 5.9 Hz), 5.87 (ddd, 2H, η^{6}-phenyl-H, $^{3}J_{H,H}$ = 5.9 Hz, 5.6 Hz, 2.1 Hz), 5.67 (d, 2H, η^{6}-phenyl-H, $^{3}J_{H,H}$ =5.9 Hz), 5.33 (t, 1H, η^{6}-phenyl-H, $^{3}J_{H,H}$ = 5.6 Hz), 4.44 (s, 6H, PTA-CH_2), 4.21 (s, 6H, PTA-CH_2), 3.97 (d, 2H, -CH_2-NH, $^{3}J_{H,H}$ = 5.9 Hz), 1.88 (s, 3H, -CH_3). ^{31}P{^{1}H} NMR (202.44 MHz; DMSO-d^{6}): -31.4 (s) ppm.

Table S1. Crystal data and details of data collection for **1** and **3**.

Complex	**1**	**3**
CCDC no.	972667	972668
Empirical formula	$C_{14}H_{26}Cl_3N_4OPRu$	$C_{15}H_{23}Cl_2N_4OPRu$
Fw	504.78	478.31
Crystal system	monoclinic	triclinic
Space group	$P2_1/n$	P-1
a, Å	6.9163(14)	10.5379(5)
b, Å	23.660(4)	12.8283(6)
c, Å	11.8396(19)	13.7451(7)
α, deg	90	100.766(2)
β, deg	97.078(9)	97.279(2)
γ, deg	90	91.491(2)
V, Å^3	1922.6(6)	1808.34(15)
Z	4	4
λ, Å	0.71073	0.71073
$\rho_{calcd,}$ g cm^{-3}	1.740	1.757
Crystal size, mm^3	0.30 × 0.05 × 0.02	0.20 × 0.08 × 0.03
T, K	100(2)	100(2)
μ, cm^{-1}	1.326	1.262
Reflns collected/unique	46451/3479	80118/10580
[R_{int}]	0.2078	0.0489
$R1$[a]	0.0548	0.0203
$wR2$[b]	0.1242	0.0505
GOF[c]	0.979	1.036

[a] $R_1 = \Sigma||Fo| - |Fc||/\Sigma|Fo|$, [b] $wR_2 = \{\Sigma w(Fo^2 - Fc^2)^2/\Sigma w(Fo^2)^2\}^{1/2}$. [c] GOF = $\{\Sigma[w(Fo^2 - Fc^2)^2]/(n - p)^{1/2}$, where n is the number of reflections and p is the total number of parameters refined.

Table S2. Key bond lengths and angles observed in the molecular structures of **1**, **3**[b] and RAPTA-C.

Bond lengths (Å) and angles (°)	**1**	**3**	**RAPTA-C**[a]
Ru–arene$_{centroid}$ / Å	1.700	1.699	1.692
Ru–C$_{substituted}$ / Å	2.198(6)	2.2834(14)	2.207(10)
			2.194(10)
Ru–C$_{unsubstituted}$ / Å	2.189(6)	2.168(2)	2.179(9)
	2.195(6)	2.175(2)	2.182(10)
	2.201(7)	2.181(2)	2.210(10)
	2.213(7)	2.187(2)	2.240(10)
	2.267(6)	2.2659(14)	
Ru–Cl1 / Å	2.432(2)	2.3966(4)	2.412(3)
Ru-Cl2 / Å	2.414(2)	2.4291(4)	2.429(2)
Ru–P1 / Å	2.307(2)	2.2916(4)	2.296(2)
P1–Ru–Cl1 / °	82.28(6)	87.477(13)	87.09(9)
P1–Ru–Cl2 / °	84.60(6)	82.730(13)	83.42(8)
Cl1–Ru–Cl2 / °	88.55(6)	88.068(13)	87.25(8)

[a] taken from Cambridge Structural Database, CCDC no. 161466

[b] data for one of two independent molecules is given.

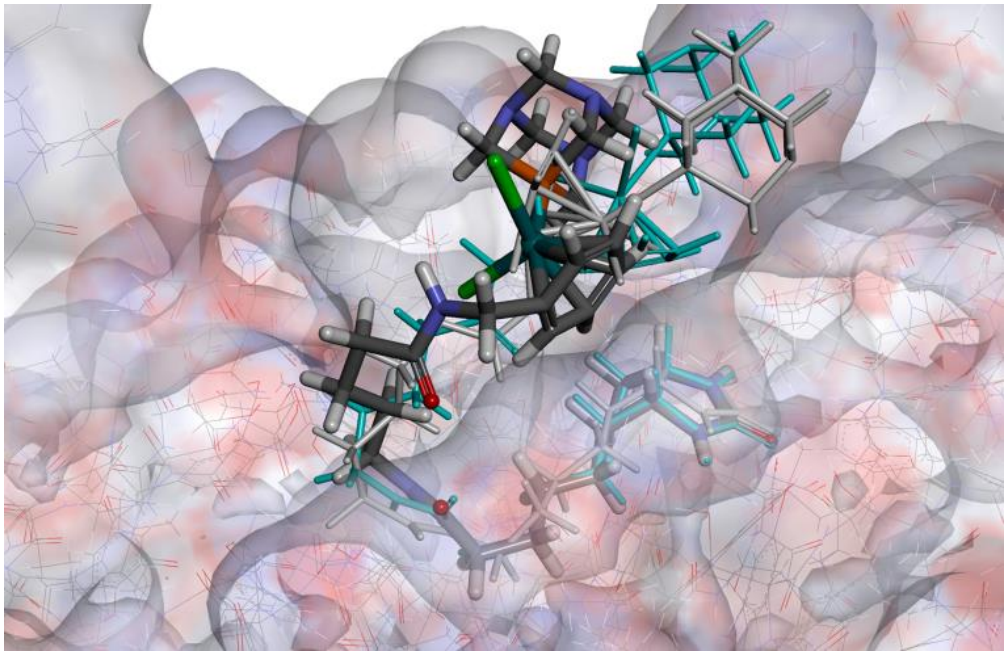

Figure S1. Docked configurations of ruthenium derivative 2 in the binding site of streptavidin for the three highest scoring GS runs overlaid. The biotin moiety shows good overlap with biotin observed in the crystal structure of the conjugate and the RAPTA part is flexible and accessible at the protein surface.

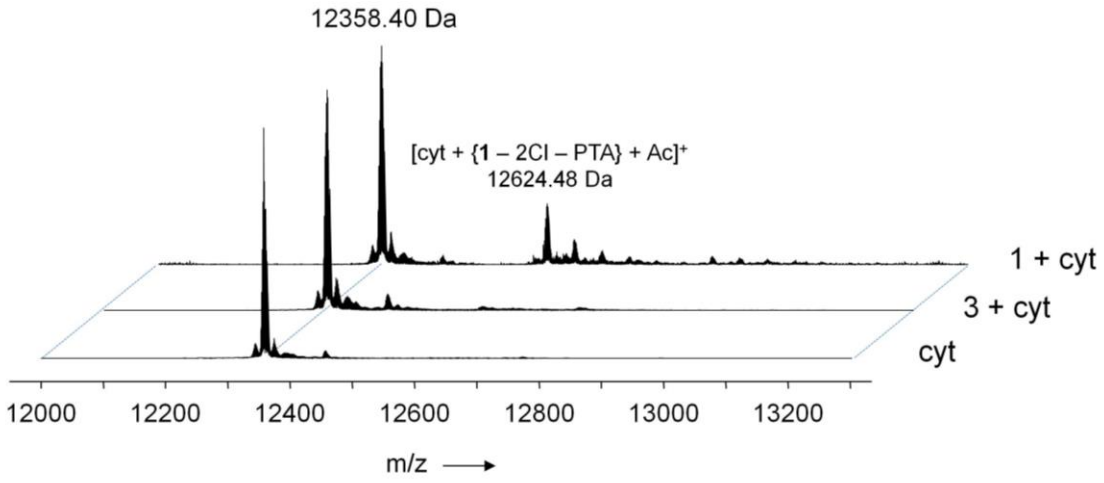

Figure S2. Deconvoluted mass spectra of incubation mixtures containing cytochrome c and **1** or **3** (molar ratio of 1 : 3) in tetramethylammonium acetate after 24 h.

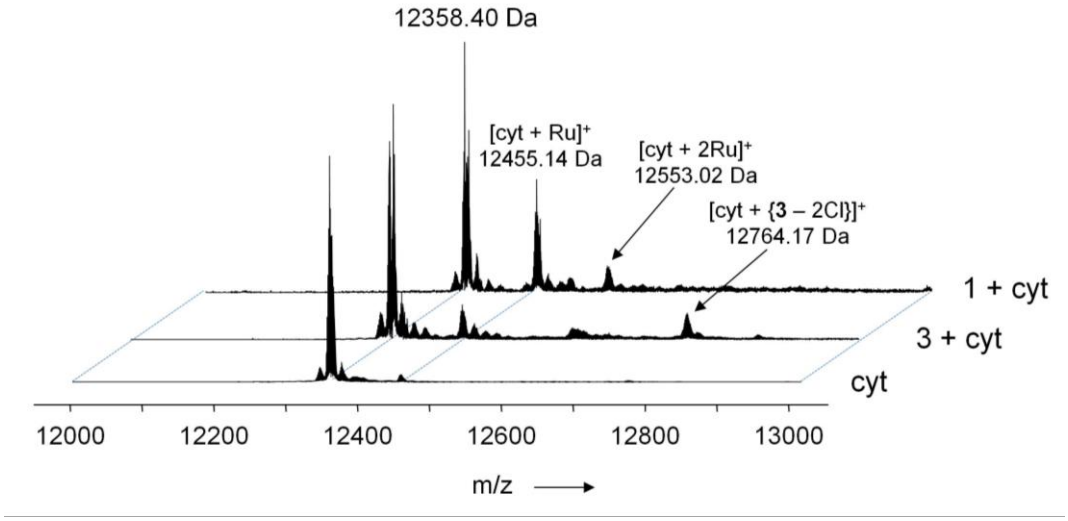

Figure S3. Deconvoluted mass spectra of aqueous incubation mixtures (pH 6.0) containing cytochrome c and **1** or **3** (molar ratio of 1 : 3) after 48 h.

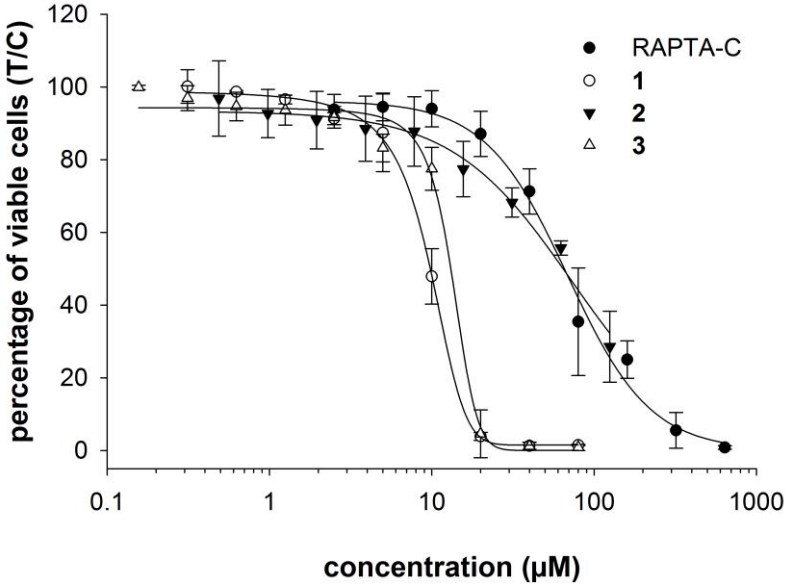

Figure S4. Concentration–effect curves of complexes **1–3** in the human ovarian cancer cell line CH1. Values were obtained by the MTT assay and are means ± standard deviations from at least three independent experiments using exposure times of 96 h.

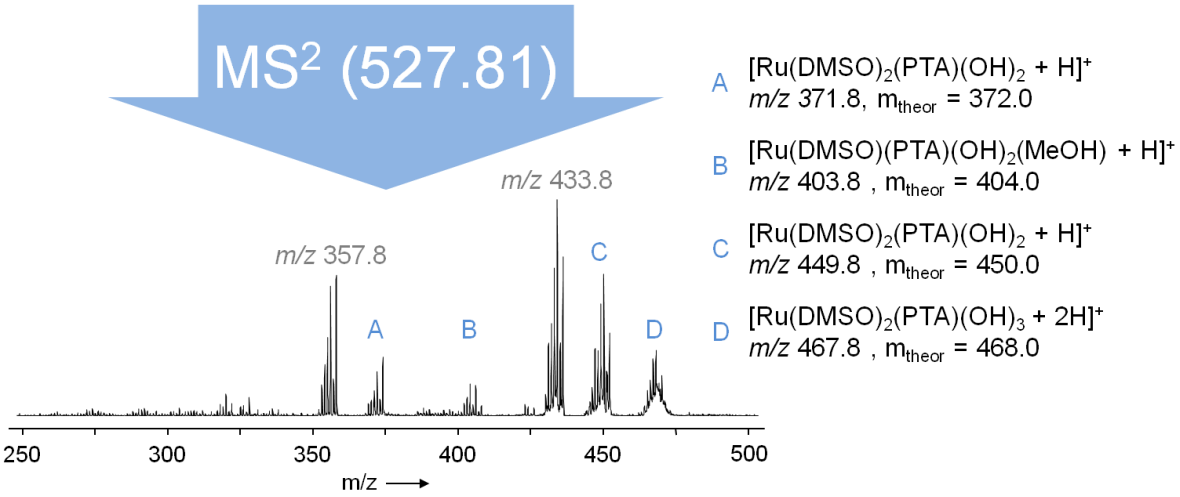

Figure S5. ESI-IT tandem mass spectrometric analysis of the signal at *m/z* 527.81 from a solution of **1** in dimethylsulfoxide after 24 h.

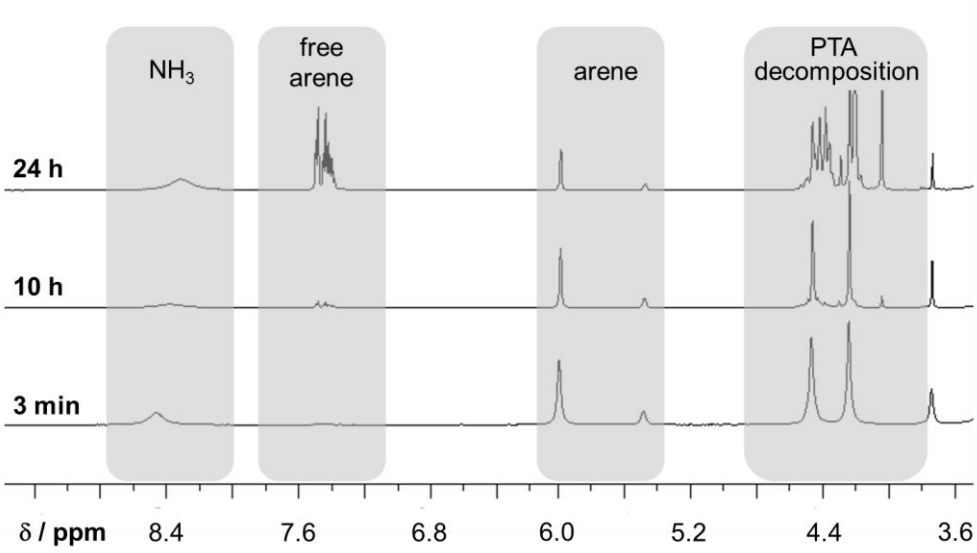

Figure S6. Time-dependent ^{1}H NMR study on the stability of **1** in dimethylsulfoxide-d^6 at room temperature.

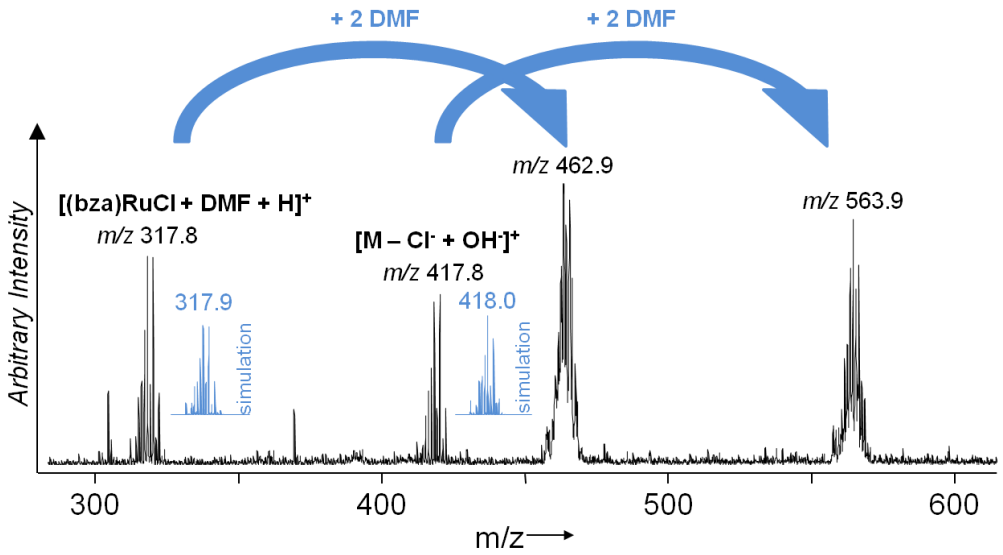

Figure S7. ESI-IT mass spectrum of a solution of **1** in dry dimethylformamide after 24 h. The solution was diluted with water : methanol (1 : 1) prior to injection into the mass spectrometer.

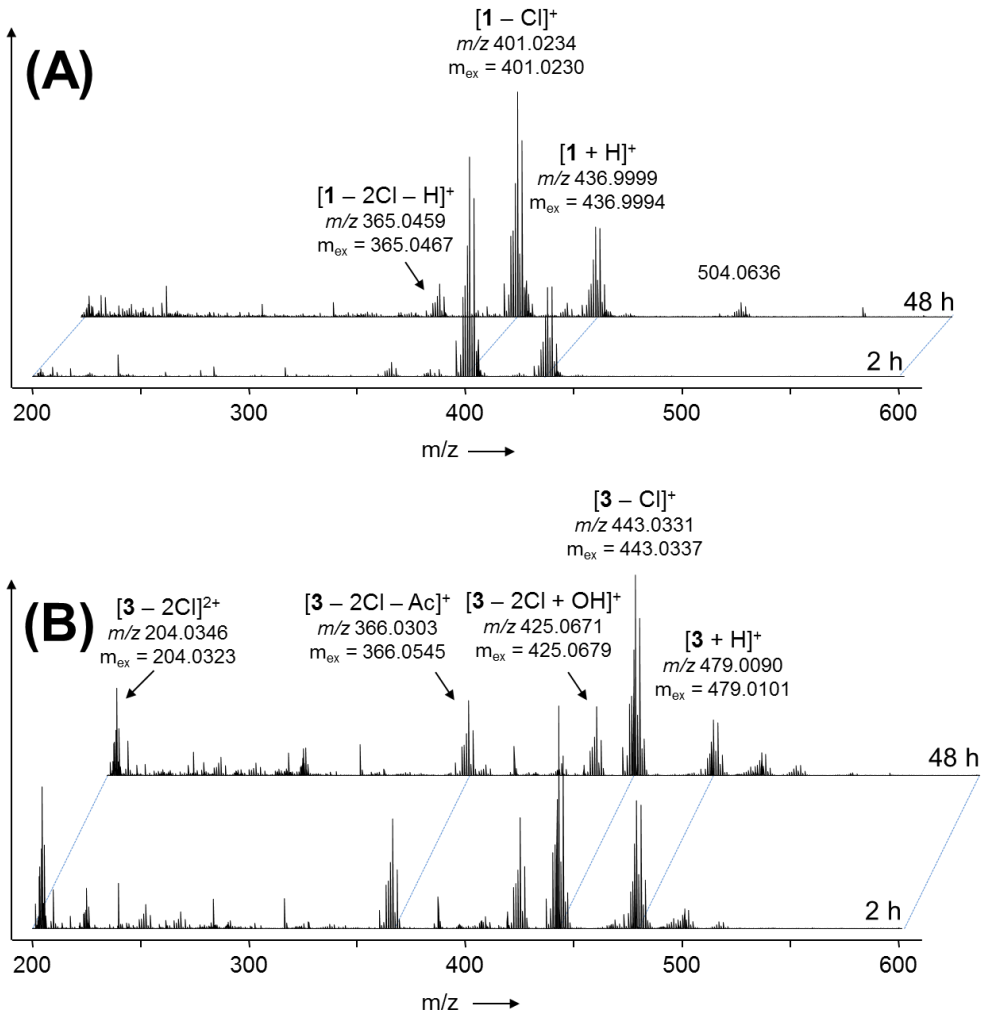

Figure S8. nESI-Q-TOF mass spectra of **1** (A) and **3** (B) in water after 2 and 48 h. The solutions were diluted with water prior to injection into the mass spectrometer.

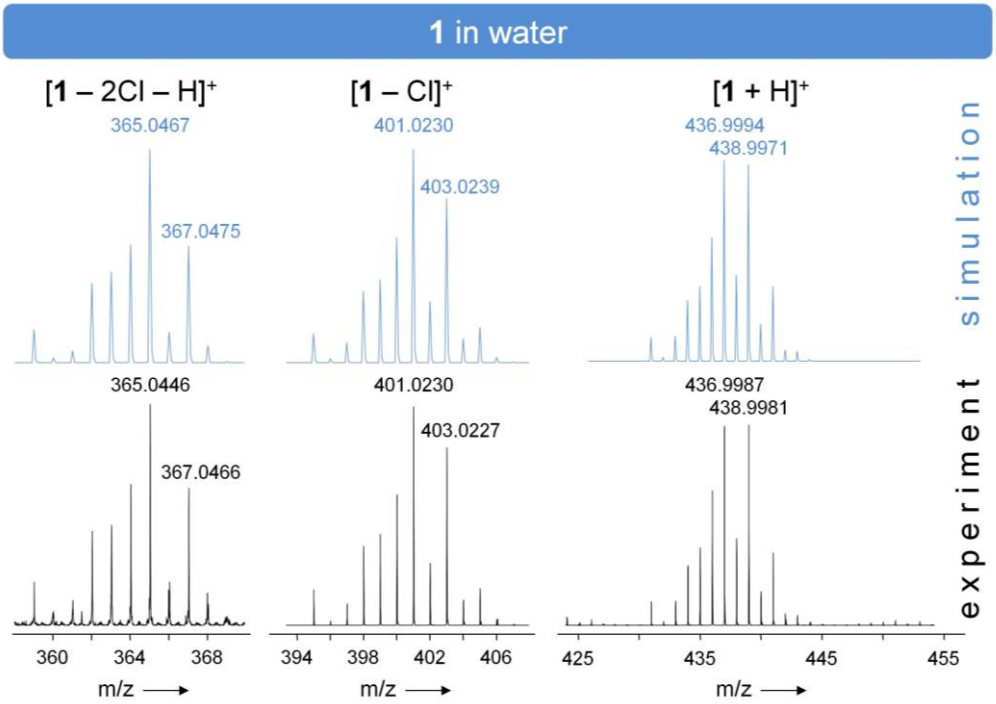

Figure S9. Experimental isotopic distributions and simulations of the mass signals of **1** in water.

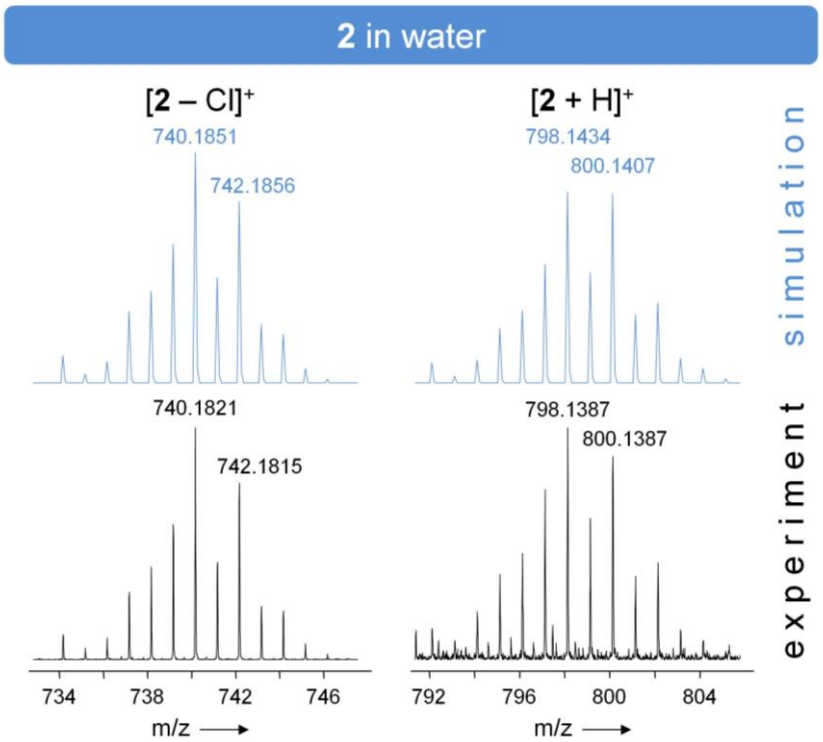

Figure S10. Experimental isotopic distributions and simulations of the mass signals of **2** in water.

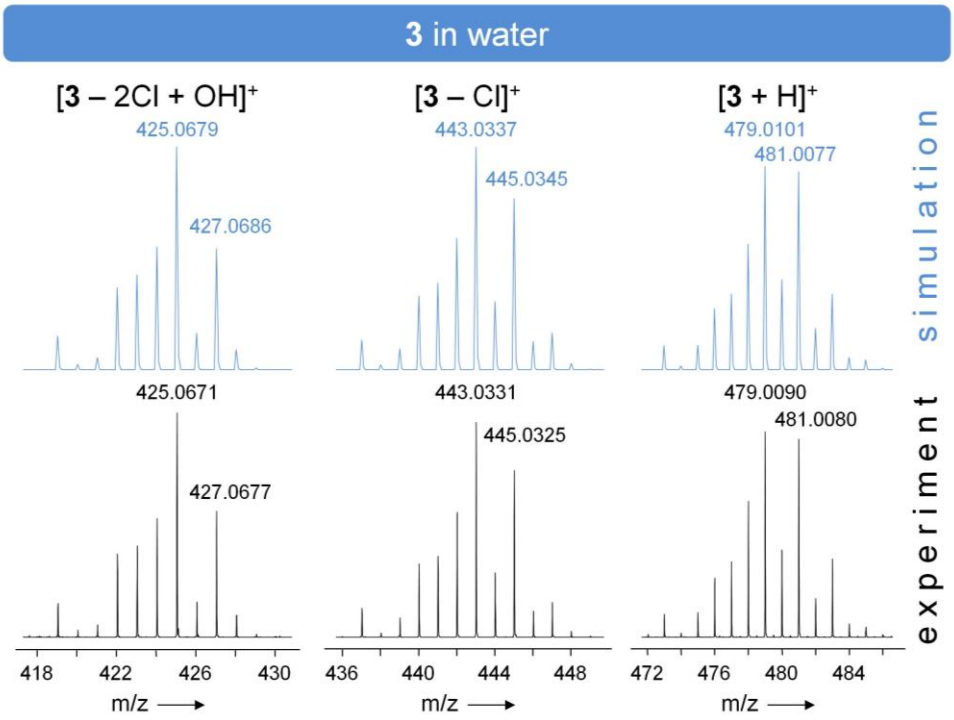

Figure S11. Experimental isotopic distributions and simulations of the mass signals of **3** in water.

Table S3. List of proteins identified by chemical proteomics. Numbers indicate spectral counts.

Protein ID	Description	Drug	Competition
RL23_HUMAN	60S ribosomal protein L23	14	14
IKBL1_HUMAN	NF-kappa-B inhibitor-like protein 1	3	7
RL29_HUMAN	60S ribosomal protein L29	13	10
ZN768_HUMAN	Zinc finger protein 768	5	2
NUMA1_HUMAN	Nuclear mitotic apparatus protein 1	10	12
HSP76_HUMAN	Heat shock 70 kDa protein 6	4	5
CLAP1_HUMAN	CLIP-associating protein 1	3	6
CMS1_HUMAN	Protein CMSS1	3	5
KIF1B_HUMAN	Kinesin-like protein KIF1B	6	6
BCD1_HUMAN	Box C/D snoRNA protein 1	4	3
SETX_HUMAN	Probable helicase senataxin	5	5
DBPA_HUMAN	DNA-binding protein A	4	5
ZEB2_HUMAN	Zinc finger E-box-binding homeobox 2	4	4
RL18_HUMAN	60S ribosomal protein L18	4	6
VIR_HUMAN	Protein virilizer homolog	3	0
RM34_HUMAN	39S ribosomal protein L34, mitochondrial	4	5
RRP1B_HUMAN	Ribosomal RNA processing protein 1 homolog B	4	1
RL27_HUMAN	60S ribosomal protein L27	5	6
H15_HUMAN	Histone H1.5	5	3
PTH_HUMAN	Probable peptidyl-tRNA hydrolase	5	4
NXF1_HUMAN	Nuclear RNA export factor 1	0	5
RIF1_HUMAN	Telomere-associated protein RIF1	4	4
HSP71_HUMAN	Heat shock 70 kDa protein 1A/1B	4	5
MK_HUMAN	Midkine	6	2
TIF1B_HUMAN	Transcription intermediary factor 1-beta	0	5
TB10B_HUMAN	TBC1 domain family member 10B	4	2
T2FA_HUMAN	General transcription factor IIF subunit 1	8	9
LS14B_HUMAN	Protein LSM14 homolog B	5	6
ZN625_HUMAN	Zinc finger protein 625	4	6
RS16_HUMAN	40S ribosomal protein S16	5	4
ZN589_HUMAN	Zinc finger protein 589	4	5
NOM1_HUMAN	Nucleolar MIF4G domain-containing protein 1	5	2
PESC_HUMAN	Pescadillo homolog	3	5
PTRF_HUMAN	Polymerase I and transcript release factor	11	11
RS19_HUMAN	40S ribosomal protein S19	6	4
RM36_HUMAN	39S ribosomal protein L36, mitochondrial	7	8
UTP11_HUMAN	Probable U3 small nucleolar RNA-associated protein 11	3	0
MET17_HUMAN	Methyltransferase-like protein 17, mitochondrial	2	6
AGRIN_HUMAN	Agrin	5	4
ZN281_HUMAN	Zinc finger protein 281	5	5
IF2G_HUMAN	Eukaryotic translation initiation factor 2 subunit 3	0	4
OZF_HUMAN	Zinc finger protein OZF	5	5
PSB5_HUMAN	Proteasome subunit beta type-5	0	6
TCP4_HUMAN	Activated RNA polymerase II transcriptional coactivator p15	4	5
FA32A_HUMAN	Protein FAM32A	4	0
H31_HUMAN	Histone H3.1	4	1
BLM_HUMAN	Bloom syndrome protein	0	2
UBP37_HUMAN	Ubiquitin carboxyl-terminal hydrolase 37	1	4
RM15_HUMAN	39S ribosomal protein L15, mitochondrial	0	2
RUFY2_HUMAN	RUN and FYVE domain-containing protein 2	2	0

Table S3. Continued

DDX47_HUMAN	Probable ATP-dependent RNA helicase DDX47	2	5
SPT5H_HUMAN	Transcription elongation factor SPT5	2	4
RL21_HUMAN	60S ribosomal protein L21	0	2
SRFB1_HUMAN	Serum response factor-binding protein 1	4	2
RAM_HUMAN	RNMT-activating mini protein	0	2
MET15_HUMAN	Probable methyltransferase-like protein 15	2	4
NOP2_HUMAN	Putative ribosomal RNA methyltransferase NOP2	0	2
AFG32_HUMAN	AFG3-like protein 2	0	2
JPH1_HUMAN	Junctophilin-1	2	2
MYL6B_HUMAN	Myosin light chain 6B	0	2
SAMD1_HUMAN	Atherin	5	5
DDX49_HUMAN	Probable ATP-dependent RNA helicase DDX49	0	2
C2D1A_HUMAN	Coiled-coil and C2 domain-containing protein 1A	2	2
ZN248_HUMAN	Zinc finger protein 248	2	2
ZC3H3_HUMAN	Zinc finger CCCH domain-containing protein 3	0	2
SNUT2_HUMAN	U4/U6.U5 tri-snRNP-associated protein 2	1	2
SC24A_HUMAN	Protein transport protein Sec24A	2	5
NOG1_HUMAN	Nucleolar GTP-binding protein 1	0	2
HXA5_HUMAN	Homeobox protein Hox-A5	3	3
PLK1_HUMAN	Serine/threonine-protein kinase PLK1	0	2
SNUT1_HUMAN	U4/U6.U5 tri-snRNP-associated protein 1	4	6
RL19_HUMAN	60S ribosomal protein L19	4	4
ALKB2_HUMAN	Alpha-ketoglutarate-dependent dioxygenase alkB homolog 2	0	2
GTPBA_HUMAN	GTP-binding protein 10	0	3
FOXK1_HUMAN	Forkhead box protein K1	2	0
ATPO_HUMAN	ATP synthase subunit O, mitochondrial	1	3
HSPB1_HUMAN	Heat shock protein beta-1	1	4
GRP75_HUMAN	Stress-70 protein, mitochondrial	2	3
CLAP2_HUMAN	CLIP-associating protein 2	3	5
TAOK2_HUMAN	Serine/threonine-protein kinase TAO2	0	2
PHF6_HUMAN	PHD finger protein 6	2	4
UIF_HUMAN	UAP56-interacting factor	4	2
CC124_HUMAN	Coiled-coil domain-containing protein 124	4	4
CDK13_HUMAN	Cyclin-dependent kinase 13	0	3
NEUA_HUMAN	N-acylneuraminate cytidylyltransferase	1	2
CHD7_HUMAN	Chromodomain-helicase-DNA-binding protein 7	4	3
MAP2_HUMAN	Microtubule-associated protein 2	1	4
CGBP1_HUMAN	CGG triplet repeat-binding protein 1	2	0
FGFP3_HUMAN	Fibroblast growth factor-binding protein 3	2	0
RS17_HUMAN	40S ribosomal protein S17	4	0
CR021_HUMAN	UPF0711 protein C18orf21	2	4
FBRL_HUMAN	rRNA 2'-O-methyltransferase fibrillarin	2	0
HMGA2_HUMAN	High mobility group protein HMGI-C	0	2
PTN_HUMAN	Pleiotrophin	5	3
RL39_HUMAN	60S ribosomal protein L39	21	15
MO4L2_HUMAN	Mortality factor 4-like protein 2	2	2
SPT2_HUMAN	Protein SPT2 homolog	4	2
KLF12_HUMAN	Krueppel-like factor 12	2	4
MBB1A_HUMAN	Myb-binding protein 1A	3	3
CENPV_HUMAN	Centromere protein V	6	6
THAP4_HUMAN	THAP domain-containing protein 4	4	4
HUTU_HUMAN	Urocanate hydratase	2	0
T53I2_HUMAN	Tumor protein p53-inducible nuclear protein 2	2	2
CHM4B_HUMAN	Charged multivesicular body protein 4b	2	0

Table S3. Continued

SOX15_HUMAN	Protein SOX-15	0	2
MA7D3_HUMAN	MAP7 domain-containing protein 3	2	0
GNL3_HUMAN	Guanine nucleotide-binding protein-like 3	2	0
H2A1B_HUMAN	Histone H2A type 1-B/E	2	4
ZN644_HUMAN	Zinc finger protein 644	0	2
TR112_HUMAN	tRNA methyltransferase 112 homolog	4	4
CC152_HUMAN	Coiled-coil domain-containing protein 152	2	3
CE152_HUMAN	Centrosomal protein of 152 kDa	0	2
CD11B_HUMAN	Cyclin-dependent kinase 11B	0	3
CENPV_HUMAN	Centromere protein V	7	6
PLCD3_HUMAN	1-phosphatidylinositol 4,5-bisphosphate phosphodiesterase delta-3	0	2
ETV3_HUMAN	ETS translocation variant 3	0	2
RL18A_HUMAN	60S ribosomal protein L18a	2	4
ZN771_HUMAN	Zinc finger protein 771	0	4
ZN182_HUMAN	Zinc finger protein 182	0	2
ARH40_HUMAN	Rho guanine nucleotide exchange factor 40	0	3
RBM42_HUMAN	RNA-binding protein 42	2	3
PIAS2_HUMAN	E3 SUMO-protein ligase PIAS2	2	3
TSR1_HUMAN	Pre-rRNA-processing protein TSR1 homolog	1	3
RS20_HUMAN	40S ribosomal protein S20	2	0
ARRD1_HUMAN	Arrestin domain-containing protein 1	1	0
GFAP_HUMAN	Glial fibrillary acidic protein	2	1
SALL4_HUMAN	Sal-like protein 4	4	4
CHM2B_HUMAN	Charged multivesicular body protein 2b	2	1
NACA_HUMAN	Nascent polypeptide-associated complex subunit alpha	3	3
ZFY27_HUMAN	Protrudin	2	2
RM22_HUMAN	39S ribosomal protein L22, mitochondrial	2	1
RT14_HUMAN	28S ribosomal protein S14, mitochondrial	0	2
ZN664_HUMAN	Zinc finger protein 664	1	2
CP087_HUMAN	UPF0547 protein C16orf87	1	1
FGF2_HUMAN	Fibroblast growth factor 2	2	2
IF2A_HUMAN	Eukaryotic translation initiation factor 2 subunit 1	1	1
ARHG2_HUMAN	Rho guanine nucleotide exchange factor 2	2	2
SHRM3_HUMAN	Protein Shroom3	2	2
SAS10_HUMAN	Something about silencing protein 10	2	2
GNA12_HUMAN	Guanine nucleotide-binding protein subunit alpha-12	0	1
PHC2_HUMAN	Polyhomeotic-like protein 2	0	1
SOST_HUMAN	Sclerostin	1	2
SPS2L_HUMAN	SPATS2-like protein	1	1
GTPB6_HUMAN	Putative GTP-binding protein 6	0	1
DDX54_HUMAN	ATP-dependent RNA helicase DDX54	1	1
AROS_HUMAN	Active regulator of SIRT1	2	2
LN28A_HUMAN	Protein lin-28 homolog A	1	0
PDIA1_HUMAN	Protein disulfide-isomerase	0	2
SP9_HUMAN	Transcription factor Sp9	1	0
RMTL1_HUMAN	RNA methyltransferase-like protein 1	1	0
ZN655_HUMAN	Zinc finger protein 655	1	0
CDC42_HUMAN	Cell division control protein 42 homolog	2	2
TAF6L_HUMAN	TAF6-like RNA polymerase II p300/CBP-associated factor-associated factor 65 kDa subunit 6L	1	0
SIR7_HUMAN	NAD-dependent protein deacetylase sirtuin-7	0	1
TCF7_HUMAN	Transcription factor 7	1	1
RS29_HUMAN	40S ribosomal protein S29	1	0

Table S3. Continued

CHTOP_HUMAN	Chromatin target of PRMT1 protein	0	1
DDX3X_HUMAN	ATP-dependent RNA helicase DDX3X	2	2
TSNA1_HUMAN	t-SNARE domain-containing protein 1	1	0
FCF1_HUMAN	rRNA-processing protein FCF1 homolog	1	2
ZN581_HUMAN	Zinc finger protein 581	1	2
LRC41_HUMAN	Leucine-rich repeat-containing protein 41	1	0
CCDC8_HUMAN	Coiled-coil domain-containing protein 8	0	1
HMGN1_HUMAN	Non-histone chromosomal protein HMG-14	1	0
CA174_HUMAN	UPF0688 protein C1orf174	2	3
PRPK_HUMAN	TP53-regulating kinase	0	2
NEP1_HUMAN	Ribosomal RNA small subunit methyltransferase NEP1	2	1
OTUD4_HUMAN	OTU domain-containing protein 4	2	0
NACC2_HUMAN	Nucleus accumbens-associated protein 2	0	2
MCES_HUMAN	mRNA cap guanine-N7 methyltransferase	0	1
RT23_HUMAN	28S ribosomal protein S23, mitochondrial	1	1
RL13A_HUMAN	60S ribosomal protein L13a	1	1
IMA2_HUMAN	Importin subunit alpha-2	0	1
SERF2_HUMAN	Small EDRK-rich factor 2	0	1
RT09_HUMAN	28S ribosomal protein S9, mitochondrial	0	1
RLA2_HUMAN	60S acidic ribosomal protein P2	1	1
PLEC_HUMAN	Plectin	1	2
PTMS_HUMAN	Parathymosin	0	1
IRS2_HUMAN	Insulin receptor substrate 2	0	2
ZNF8_HUMAN	Zinc finger protein 8	0	1
ERI1_HUMAN	3'-5' exoribonuclease 1	0	1
ANKZ1_HUMAN	Ankyrin repeat and zinc finger domain-containing protein 1	2	1
GULP1_HUMAN	PTB domain-containing engulfment adapter protein 1	1	2
BPTF_HUMAN	Nucleosome-remodeling factor subunit BPTF	1	0

References

1 F. K. Cheung, C. Lin, F. Minissi, A. L. Crivillé, M. A. Graham, D. J. Fox and M. Wills, *Org. Lett.*, 2007, **9**, 4659-4662.

2 W. H. Ang, E. Daldini, L. Juillerat-Jeanneret and P. J. Dyson, *Inorg. Chem.*, 2007, **46**, 9048-9050.

3 D. J. Daigle, A. B. Pepperman and S. L. Vail, *J. Heterocycl. Chem.*, 1974, **11**, 407-408.

4 M. R. Pressprich and J. Chambers, Bruker Analytical X-ray systems, Madison, 2004.

5 G. M. Sheldrick, *Acta Crystallogr., Sect. A: Found. Crystallogr.*, 2008, **A64**, 112-122.

6 O. V. Dolomanov, L. J. Bourhis, R. J. Gildea, J. A. K. Howard and H. Puschmann, *J. Appl. Crystallogr.*, 2009, **42**, 339-341.

7 I. Le Trong, Z. Wang, D. E. Hyre, T. P. Lybrand, P. S. Stayton and R. E. Stenkamp, *Acta Crystallogr. Sect. D*, 2011, **67**, 813-821

8 H. M. Berman, J. Westbrook, Z. Feng, G. Gilliland, T. N. Bhat, H. Weissig, I. N. Shindyalov and P. E. Bourne, *Nuc.Acids Res.*, 2000, **28**, 235-242.

9 H. Berman, K. Henrick and H. Nakamura, *Nat. Struct. Biol.*, 2003, **10**, 980.

10 Fijitsu Limited, 2000 - 2007.

11 N. L. Allinger, *J. Am. Chem. Soc.*, 1977, **99**, 8127-8134.

12 G. Jones, P. Willet, R. C. Glen, A. R. Leach and R. Taylor, *J.Mol.Biol.*, 1997, **267**, 727-748.

13 M. D. Eldridge, C. Murray, T. R. Auton, G. V. Paolini and P. M. Mee, *J. Comp. Aid. Mol. Design*, 1997, **11**, 425-445.

14 M. L. Verdonk, J. C. Cole, M. J. Hartshorn, C. W. Murray and R. D. Taylor, *Proteins*, 2003, **52**, 609-623.

15 O. Korb, T. Stützle and T. E. Exner, *J. Chem. Inf. Model.*, 2009, **49**, 84-96.

16 W. T. M. Mooij and M. L. Verdonk, *Proteins*, 2005, **61**, 272-287.

17 K. L. Bennett, M. Funk, M. Tschernutter, F. P. Breitwieser, M. Planyavsky, C. U. Mohien, A. Muller, Z. Trajanoski, J. Colinge, G. Superti-Furga and U. Schmidt-Erfurth, *J. Proteomics*, 2011, **74**, 151-166.

18 J. V. Olsen, L. M. F. de Godoy, G. Q. Li, B. Macek, P. Mortensen, R. Pesch, A. Makarov, O. Lange, S. Horning and M. Mann, *Mol. Cell Proteomics*, 2005, **4**, 2010-2021.

19 J. Colinge, A. Masselot, M. Giron, T. Dessingy and J. Magnin, *Proteomics*, 2003, **3**, 1454-1463.

20 S. Naik, G. Bhattacharjya, B. Talukdar and Bhisma K. Patel, *Eur. J. Org. Chem.*, 2004, **2004**, 1254-1260.